



HAL
open science

Estimation of the Error in the Calculation of the Pressure-Strain Term: Application in the Terrestrial Magnetosphere

O. W. Roberts, Z. Vörös, K. Torkar, J. Stawarz, R. Bandyopadhyay, D. J. Gershman, Y. Narita, R. Kieokaew, B. Lavraud, K. Klein, et al.

► To cite this version:

O. W. Roberts, Z. Vörös, K. Torkar, J. Stawarz, R. Bandyopadhyay, et al.. Estimation of the Error in the Calculation of the Pressure-Strain Term: Application in the Terrestrial Magnetosphere. *Journal of Geophysical Research: Space Physics*, 2023, 128, 10.1029/2023JA031565 . insu-04473166

HAL Id: insu-04473166

<https://insu.hal.science/insu-04473166v1>

Submitted on 13 Mar 2024

HAL is a multi-disciplinary open access archive for the deposit and dissemination of scientific research documents, whether they are published or not. The documents may come from teaching and research institutions in France or abroad, or from public or private research centers.

L'archive ouverte pluridisciplinaire **HAL**, est destinée au dépôt et à la diffusion de documents scientifiques de niveau recherche, publiés ou non, émanant des établissements d'enseignement et de recherche français ou étrangers, des laboratoires publics ou privés.

Copyright

JGR Space Physics

METHOD

10.1029/2023JA031565

Key Points:

- We estimate the errors on the pressure strain terms calculated from Magnetospheric MultiScale Mission data
- The errors are estimated using two methods, standard error propagation from the velocity and temperature errors and a Monte Carlo method
- Two applications are given using Magnetospheric MultiScale Mission data at the magnetopause and in the magnetotail of Earth

Correspondence to:










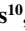

O. W. Roberts,
owen.roberts@oew.ac.at

Citation:

Roberts, O. W., Vörös, Z., Torkar, K., Stawarz, J., Bandyopadhyay, R., Gershman, D. J., et al. (2023). Estimation of the error in the calculation of the pressure-strain term: Application in the terrestrial magnetosphere. *Journal of Geophysical Research: Space Physics*, 128, e2023JA031565. <https://doi.org/10.1029/2023JA031565>

Received 7 APR 2023
Accepted 28 JUL 2023

Estimation of the Error in the Calculation of the Pressure-Strain Term: Application in the Terrestrial Magnetosphere

O. W. Roberts¹ , Z. Vörös^{1,2} , K. Torkar¹ , J. Stawarz³, R. Bandyopadhyay⁴ , D. J. Gershman⁵ , Y. Narita¹ , R. Kieokaew⁶ , B. Lavraud^{6,7} , K. Klein⁸ , Y. Yang⁹, R. Nakamura¹ , A. Chasapis¹⁰, and W. H. Matthaeus⁹ 

¹Space Research Institute, Austrian Academy of Sciences, Graz, Austria, ²Institute of Earth's Physics and Space Science, ELRN, Sopron, Hungary, ³Department of Mathematics, Physics and Electrical Engineering, Northumbria University, Newcastle upon Tyne, UK, ⁴Department of Astrophysical Sciences, Princeton University, Princeton, NJ, USA, ⁵NASA Goddard Space Flight Center, Greenbelt, MD, USA, ⁶Institut de Recherche en Astrophysique et Planétologie, CNRS, UPS, CNES, Université de Toulouse, Toulouse, France, ⁷Laboratoire d'Astrophysique de Bordeaux, CNRS, University of Bordeaux, Pessac, France, ⁸Lunar and Planetary Laboratory, University of Arizona, Tucson, AZ, USA, ⁹Department of Physics and Astronomy and Bartol Research Institute, University of Delaware, Newark, DE, USA, ¹⁰Laboratory for Atmospheric and Space Physics, University of Colorado Boulder, Boulder, CO, USA

Abstract Calculating the pressure-strain terms has recently been performed to quantify energy conversion between the bulk flow energy and the internal energy of plasmas. It has been applied to numerical simulations and satellite data from the Magnetospheric MultiScale Mission. The method requires spatial gradients of the velocity and the use of the full pressure tensor. Here we present a derivation of the errors associated with calculating the pressure-strain terms from multi-spacecraft measurements and apply it to previously studied examples of magnetic reconnection at the magnetopause and the magnetotail. The errors are small in a dense magnetosheath event but much larger in the more tenuous magnetotail. This is likely due to larger counting statistics in the dense plasma at the magnetopause than in the magnetotail. The propagated errors analyzed in this work are important to understand uncertainties of energy conversion measurements in space plasmas and have applications to current and future multi-spacecraft missions.

1. Introduction

Space plasma processes are often inherently three-dimensional, and single-point measurements cannot distinguish between spatial and temporal changes. Therefore, to better understand space plasma phenomena, multi-point missions such as Cluster (Escoubet et al., 1997, 2001), the Time History of Events and Macroscale Interactions during Substorms (THEMIS) (Angelopoulos, 2008), Swarm (Friis-Christensen et al., 2008), the Magnetospheric MultiScale Mission (MMS) (Burch et al., 2016), and HelioSwarm (Klein et al., 2019) were conceived. Along with the missions, several multi-point methods were developed (M. Dunlop et al., 1988; Paschmann, 1998; Paschmann & Daly, 2008). These include multi-spacecraft wave analysis methods (Constantinescu, 2007; Dudok de Wit et al., 1995; Glassmeier et al., 2001; Motschmann et al., 1996; Narita et al., 2010, 2011, 2021; Pincon & Lefeuvre, 1991; Roberts et al., 2014, 2017; Vogt, Narita, & Constantinescu, 2008), multi-point structure functions (Chen et al., 2010; Pecora et al., 2023; Roberts et al., 2022), multi-point correlation functions (Bandyopadhyay, Matthaeus, Chasapis, et al., 2020; Horbury, 2000; Matthaeus et al., 2005; K. T. Osman & Horbury, 2007; K. Osman & Horbury, 2009), and magnetic field reconstruction (Broeren et al., 2021; Denton et al., 2020, 2022).

Tetrahedral configurations used on Cluster and MMS allow the calculation of spatial gradients and curls in the plasma. The current density can be estimated by calculating the curl of the magnetic field. This method is termed the curlometer method (M. Dunlop et al., 1988; M. W. Dunlop et al., 2002; Perri et al., 2017; M. W. Dunlop et al., 2021). The curlometer method has often been applied to Cluster magnetic field (M. W. Dunlop et al., 2002; Perrone et al., 2016, 2017; M. W. Dunlop et al., 2021), and velocity data (Kieokaew & Foullon, 2019) where some assumptions are required as ion data is not available on all spacecraft. The curlometer method has also been applied to MMS magnetic field data (Gershman et al., 2018; Lavraud et al., 2016; Phan et al., 2016; Wang et al., 2019). The MMS spacecraft provides multi-point magnetic field data and high-time resolution plasma data,

which allows comparison of the curlometer current to the current measured from the plasma data (Gershman et al., 2018; Lavraud et al., 2016; Phan et al., 2016). The multi-point high-time resolution of plasma data has also allowed calculations of the vorticity using the full four spacecraft plasma data (Wang et al., 2019; Zhang et al., 2020).

The plasma heating and energization mechanisms are crucial to understanding several processes, such as plasma turbulence and reconnection. Because of the spatiotemporal ambiguity, it is not always apparent whether temperature increases are due to changing environments, for example, crossing into a hotter region rather than local heating. The pressure-strain methodology (Bandyopadhyay, Matthaeus, Parashar, et al., 2020; Cassak & Barbhuiya, 2022; Chasapis et al., 2018; Del Sarto et al., 2016; Del Sarto & Pegoraro, 2018; Fadanelli et al., 2021; Matthaeus, 2021; Matthaeus et al., 2020; Pezzi et al., 2019; Vörös et al., 2023; Wang et al., 2019; Yang et al., 2022; Yang, Matthaeus, Parashar, Haggerty, et al., 2017; Yang, Matthaeus, Parashar, Wu, et al., 2017) allows the quantification of energy conversion between the internal energy of the plasma and the bulk flow. The calculation requires multi-spacecraft velocity measurements so that the divergence and spatial gradients of the velocity field can be calculated. The method also requires measurement of the full pressure tensor. The plasma moments are derived from distribution functions comprising a finite number of measured particles. This results in the moments being affected by Poisson noise. However, an analysis of the errors associated with calculating the pressure-strain terms has not been presented.

This brief report aims to derive the equations for the error propagation for the pressure-strain terms. In the following section, we will present the Pressure-Strain methodology. The derivation of the error terms follows, and example applications to reconnection events studied by Burch et al. (2020), Lu et al. (2020), and Bandyopadhyay et al. (2021) are presented.

2. Pressure-Strain Methodology

The system of equations governing energy conversion in plasmas is given below. These are obtained from manipulating the Maxwell-Vlasov equations (Bandyopadhyay et al., 2021; Birn & Hesse, 2005, 2010; Cerri et al., 2016; Chasapis et al., 2018; Fadanelli et al., 2021; Matthaeus, 2021; Yang, Matthaeus, Parashar, Haggerty, et al., 2017; Yang, Matthaeus, Parashar, Wu, et al., 2017).

$$\partial_t \mathcal{E}_s^f + \nabla \cdot (\mathcal{E}_s^f \mathbf{V}_s + \mathbf{P}_s \cdot \mathbf{V}_s) = (\mathbf{P}_s \cdot \nabla) \cdot \mathbf{V}_s + n_s q_s \mathbf{E} \cdot \mathbf{V}_s \quad (1)$$

$$\partial_t \mathcal{E}_s^{in} + \nabla \cdot (\mathcal{E}_s^{in} \mathbf{V}_s + \mathbf{h}_s) = -(\mathbf{P}_s \cdot \nabla) \cdot \mathbf{V}_s \quad (2)$$

$$\partial_t \mathcal{E}^m + \frac{c}{4\pi} \nabla \cdot (\mathbf{E} \times \mathbf{B}) = -\mathbf{J} \cdot \mathbf{E} \quad (3)$$

where, \mathcal{E}_s^f is the fluid flow energy of particle species s , \mathcal{E}^m is the electromagnetic energy and \mathcal{E}_s^{in} is the internal (or random energy). \mathbf{P}_s is the pressure tensor, \mathbf{h}_s is the heat flux vector, \mathbf{V}_s is the velocity, n_s is the number density, and q is the charge. Finally, \mathbf{E} and \mathbf{B} denote the electric and magnetic fields, and $\mathbf{J} = \sum_s \mathbf{J}_s$ is the total current density.

The divergence terms (on the left-hand side of Equations 1–3) are transport terms and move energy from one location to another. We see that the conversion of energy (right-hand side of Equations 1–3) can occur through different channels. The $\mathbf{J} \cdot \mathbf{E}$ term converts electromagnetic energy into kinetic energy, and the pressure-strain term converts energy between the internal energy and the bulk flow (Birn & Hesse, 2010; Del Sarto & Pegoraro, 2018; Del Sarto et al., 2016; Fadanelli et al., 2021; Matthaeus, 2021; Yang, Matthaeus, Parashar, Haggerty, et al., 2017; Yang, Matthaeus, Parashar, Wu, et al., 2017).

Energy conversion into the plasma's internal energy can only be quantified from the pressure-strain term $(\mathbf{P}_s \cdot \nabla) \cdot \mathbf{V}_s$. The pressure-strain term, therefore, quantifies conversions between internal and flow energies. Calculating this quantity (due to the need for spatial gradients) requires velocity measurements at multiple points and the pressure tensor. With its four spacecraft and exceptional plasma measurements, the MMS mission is ideal for applying this methodology. The pressure-strain term can be further expressed as follows (Bandyopadhyay et al., 2021; Chasapis et al., 2018; Del Sarto et al., 2016; Del Sarto & Pegoraro, 2018; Yang, Matthaeus, Parashar, Haggerty, et al., 2017)

$$-(\mathbf{P}_s \cdot \nabla) \cdot \mathbf{V}_s = -p \delta_{i,j} \partial_j u_i - (P_{i,j} - p \delta_{i,j}) \partial_j u_i = -p\theta - \Pi_{i,j} : D_{i,j} \quad (4)$$

where $p = \frac{1}{3} P_{i,i}$, $\theta = \nabla \cdot \mathbf{V}_s$ and $\Pi_{i,j} = P_{i,j} - p\delta_{i,j}$ is the traceless pressure tensor and $D_{i,j} = \frac{1}{2}(\partial_i u_j + \partial_j u_i) - \frac{1}{3}\theta\delta_{i,j}$. The delta here is the Kronecker delta. If a plasma is incompressible, $\theta = 0$ thus, $p\theta$ denotes compressible, and ΠD denotes incompressible channels for energy conversion. By measuring these quantities with MMS, we can identify regions where energy conversion occurs. However, at the MMS separations, the differences in velocity may be very small between the spacecraft. Therefore, estimating the propagation of the uncertainty in calculating velocity gradients and the error associated with the pressure tensor is prudent.

3. Error Calculation

Here we present a brief discussion of the errors in calculating the pressure-strain terms. When calculating gradients using multiple spacecraft, there are three different sources of errors. The first is the error in the measurement; in the case of a plasma measurement, this is related to the counting statistics. The second source of error is from the spacecraft positions and the timing between spacecraft. The aforementioned uncertainties will also be enhanced by the shape of the spacecraft formation (Chanteur, 1998, 2000; Vogt, Paschmann, & Chanteur, 2008; Vogt et al., 2009, 2011, 2020) if it is not regular. Finally, even in the case of a perfect tetrahedron, there can be deviations from linearity. This type of error is impossible to quantify with four-point measurements, especially if a fluctuation is nonlinear or a structure has a scale size smaller than the separations. However, for smaller spacecraft separations, this error is expected to be smaller (Vogt et al., 2020).

Plasma instruments count individual particles; consequently, there will be random errors due to Poisson noise (i.e., related to the counting statistics). The statistical errors on the moments from MMS are available in the Fast Plasma Investigation (FPI) (Pollock et al., 2016) level-2 moments. Note level-2 means the science quality, ground processed moments, where corrections have been applied because of the spacecraft potential. Details of the calculation of the statistical errors are available in Gershman et al. (2015). They are based on error propagation and consider the counts in the instrument (instrument true response), and the phase space density (calibrated instrument response).

The divergence uncertainty was investigated by Vogt and Paschmann (1998). The calculation of a divergence from four point measurements is given by;

$$\nabla \cdot \mathbf{V} \simeq \sum_{\alpha} \mathbf{k}_{\alpha} \cdot \mathbf{V}_{\alpha} \quad (5)$$

where α denotes the spacecraft \mathbf{k} is the reciprocal vector defined as;

$$\mathbf{k}_{\alpha} = \frac{\mathbf{r}_{\beta,\gamma} \times \mathbf{r}_{\beta,\lambda}}{\mathbf{r}_{\beta,\alpha} \cdot (\mathbf{r}_{\beta,\gamma} \times \mathbf{r}_{\beta,\lambda})} \quad (6)$$

where $\mathbf{r}_{\alpha,\beta} = \mathbf{r}_{\beta} - \mathbf{r}_{\alpha}$ are the relative position vectors of the four spacecraft, where $(\alpha, \beta, \gamma, \lambda)$ must be a cyclic permutation of 1, 2, 3, 4 (Chanteur, 1998; Vogt, Paschmann, & Chanteur, 2008).

The spacecraft positions are known to a value <100 m, and timing accuracy across the spacecraft is <1 ms (Tooley et al., 2016). The uncertainty from the positional and timing accuracy is negligible compared to other sources of error. We give a quantitative estimate in the appendix for the intervals used here.

Errors due to the tetrahedral shape are related to the trace of the reciprocal tensor. This is defined as $\sum_{\alpha=1}^4 |\mathbf{k}_{\alpha}|^2$, (Chanteur, 1998, 2000; Vogt et al., 2009, 2020; Vogt, Paschmann, & Chanteur, 2008). This can be considered an amplification factor for the measurement, positional, and timing errors. The analytical error amplification is a function of the planarities P and elongations E of the spacecraft constellation defined by (Robert, Roux, et al., 1998) with larger values of P and E yielding larger amplifications of the error (Chanteur, 1998, 2000; Vogt et al., 2009, 2020; Vogt, Paschmann, & Chanteur, 2008). Numerical testing of the curlometer method for different constellation planarities P and elongations E also demonstrated that when $\sqrt{P^2 + E^2} < 0.6$ the error in the current estimation was <3% and $\sqrt{P^2 + E^2} \sim 0.9$ the error was of the order of 10% (Robert, Dunlop,

et al., 1998). We can expect that the dominant error sources for the studied intervals are the particle measurement and the tetrahedron's shape.

The error in the divergence of velocity derived in Vogt and Paschmann (1998) is then given by:

$$\sigma[\nabla \cdot \mathbf{V}] \simeq \sqrt{\sum_{\alpha} (k_{\alpha}^2 \cdot \sigma[V_{\alpha}]^2)}. \quad (7)$$

here σ denotes the error of the quantity in the square brackets. Therefore the error in the compressive part of the pressure-strain term comes from a combination of the error from Equation 7 and the error in the pressure tensor $\mathbf{P}_{\text{Error}}$. Note that Equation 7 contains the error due to the shape ($\sum_{\alpha=1}^4 |k_{\alpha}|^2$) and the particle measurement ($\sum_{\alpha=1}^4 \sigma[V_{\alpha}]^2$), the dominant sources of error in our intervals. We use the equations for uncertainty propagation to estimate the combined error. We averaged the pressure tensors from the four spacecraft

$$\mathbf{P}_{\text{av}} = \frac{1}{4} \sum_{\alpha} \mathbf{P}_{\alpha}, \quad (8)$$

the associated errors on the pressure tensor elements are propagated following;

$$\sigma[P_{\text{av},i,j}] = \frac{1}{4} \sqrt{P_{1,\text{err},i,j}^2 + P_{2,\text{err},i,j}^2 + P_{3,\text{err},i,j}^2 + P_{4,\text{err},i,j}^2}, \quad (9)$$

the total pressure is given by:

$$p = \frac{1}{3} \sum_i P_{\text{av},i,i}, \quad (10)$$

and the corresponding error is:

$$\sigma[p] = \frac{1}{3} \sqrt{\sigma[P_{\text{av},x,x}]^2 + \sigma[P_{\text{av},y,y}]^2 + \sigma[P_{\text{av},z,z}]^2}. \quad (11)$$

The final error in the $p\theta$ term is given by:

$$\sigma[p\theta] = |p\theta| \sqrt{\left(\frac{\sigma[\nabla \cdot \mathbf{V}]}{\nabla \cdot \mathbf{V}}\right)^2 + \left(\frac{\sigma[p]}{p}\right)^2}. \quad (12)$$

For the calculation of a directional derivative (in the direction x_i), the errors are given by:

$$\sigma\left[\frac{\partial V_j}{\partial x_i}\right] = \sqrt{\sum_{\alpha} (k_{\alpha,i}^2 \sigma[V_{\alpha,j}]^2)}. \quad (13)$$

The errors on the off-diagonal D terms then become;

$$\sigma[D_{i,j}] = \frac{1}{2} \sqrt{\left(\sigma\left[\frac{\partial V_j}{\partial x_i}\right]^2 + \sigma\left[\frac{\partial V_i}{\partial x_j}\right]^2\right)}. \quad (14)$$

and the error for the diagonal terms D like the $\sigma[D_{x,x}]$ term becomes;

$$\sigma[D_{x,x}] = \sqrt{\left(\frac{4}{9} \sigma\left[\frac{\partial V_x}{\partial x}\right]^2 + \frac{1}{9} \sigma\left[\frac{\partial V_y}{\partial y}\right]^2 + \frac{1}{9} \sigma\left[\frac{\partial V_z}{\partial z}\right]^2\right)}. \quad (15)$$

The traceless pressure tensor's off-diagonal elements are equal to the full pressure tensor, however the diagonal elements such as $\sigma[\Pi_{x,x}]$ become;

$$\sigma[\Pi_{x,x}] = \sqrt{\frac{4}{9} \sigma[P_{\text{av},x,x}]^2 + \frac{1}{9} \sigma[P_{\text{av},y,y}]^2 + \frac{1}{9} \sigma[P_{\text{av},z,z}]^2} \quad (16)$$

Combining the errors from the traceless pressure tensor and D we obtain a combined error tensor.

$$\sigma[D_{i,j}\Pi_{i,j}] = |D_{i,j}\Pi_{i,j}| \sqrt{\left(\frac{\sigma[D_{i,j}]}{D_{i,j}}\right)^2 + \left(\frac{\sigma[\Pi_{i,j}]}{\Pi_{i,j}}\right)^2} \quad (17)$$

Only six unique error terms exist in Equation 17 because the D and the Π tensors (and their errors) are symmetric that is, $\sigma[D_{x,y}\Pi_{x,y}] = \sigma[D_{y,x}\Pi_{y,x}]$. Thus, the final error in the ΠD term is then given by:

$$\sigma[\Pi D] = \sqrt{\begin{aligned} &\sigma[D_{x,x}\Pi_{x,x}]^2 + \sigma[D_{y,y}\Pi_{y,y}]^2 + \sigma[D_{z,z}\Pi_{z,z}]^2 \\ &+ 4\sigma[D_{x,y}\Pi_{x,y}]^2 + 4\sigma[D_{x,z}\Pi_{x,z}]^2 + 4\sigma[D_{y,z}\Pi_{y,z}]^2 \end{aligned}} \quad (18)$$

For completeness, the total pressure-strain term error is given in 19.

$$\sigma_{(\mathbf{p}_s \cdot \mathbf{v}) \cdot \mathbf{v}_s} = \sqrt{\sigma[p\theta]^2 + \sigma[\Pi D]^2} \quad (19)$$

4. Application to the Terrestrial Magnetosphere

Two examples of the application of the method and the error calculation are now presented. The data are from MMS when the spacecraft were in the burst telemetry mode; magnetic field data are from the fluxgate magnetometers (Russell et al., 2016) with a sampling rate of 128 Hz. The plasma data are from the FPI instrument (Pollock et al., 2016), where the sampling rates are 6.6 Hz for ions and 30.3 Hz for electrons. Figure 1 show an example of magnetic reconnection studied by Burch et al. (2020) and later using the pressure-strain methodology by Bandyopadhyay et al. (2021). MMS was at the magnetopause in this case, and the mean electron number density was moderate 7.19 cm^{-3} . ($P = 0.56$, $E = 0.35$, $\sqrt{P^2 + E^2} = 0.67$) was not perfectly regular. To calculate the pressure-strain terms, we remove the spin effects using the spin tone product in the FPI L2 data files before calculating the gradients. We see that the errors are small, and the application of the method is justified.

Figure 2 presents a second magnetic reconnection case. This case studied previously by Lu et al. (2020) occurs in the magnetotail. Magnetotail plasma is typically much more tenuous compared to magnetosheath/magnetopause plasma. In this case, the mean electron number density is 0.58 cm^{-3} ; therefore, we expect the errors to be larger due to poor counting statistics. For this case the spacecraft constellation was regular with $P = 0.12$, $E = 0.06$, $\sqrt{P^2 + E^2} = 0.13$. The absolute errors for both cases are given in Table 1. As expected, the absolute errors in the magnetotail are significantly larger than at the magnetopause.

We perform a statistical Monte Carlo test on the data to provide an additional estimate of the error. We take the individual velocity and pressure tensor series and their respective errors and compute 100 new time series. This is performed by adding a random (Gaussian distributed) error with a mean of zero and a standard deviation equal to the statistical error to the measured velocity and pressure tensor components. We perform this procedure one hundred times and calculate the pressure strain terms with each of our realizations of the time series. We calculate the standard deviation from the 100 realizations for each point, yielding another estimation. This analysis is presented in Figures 3 and 4. The standard deviation of the one hundred time series agrees well with those estimated through the equations given in the previous section, giving further confidence in the error estimation and the technique itself. We also present the averages of the absolute errors in Table 1.

To better understand the limitations of the method in different regions that MMS surveys, we plot the electron number density (Figure 5a) and the relative errors on the ion (Figure 5b) and electron bulk speeds (Figure 5c) as a function of the spacecraft position in the xy GSE plane in the year 2018. Here we see that the errors are significantly larger in the magnetotail where the density is lower. The relative errors on the electron bulk velocities are also larger than those of the ions; this is possibly due to the effects of photoelectrons (Gershman et al., 2017; Lavraud & Larson, 2016), which are removed using a model from the L2 data, which may cause larger uncertainties, especially when counts are already low. Therefore we would urge caution when using the method in low-density regions. It should be noted that the error in the pressure tensor components, is also important for

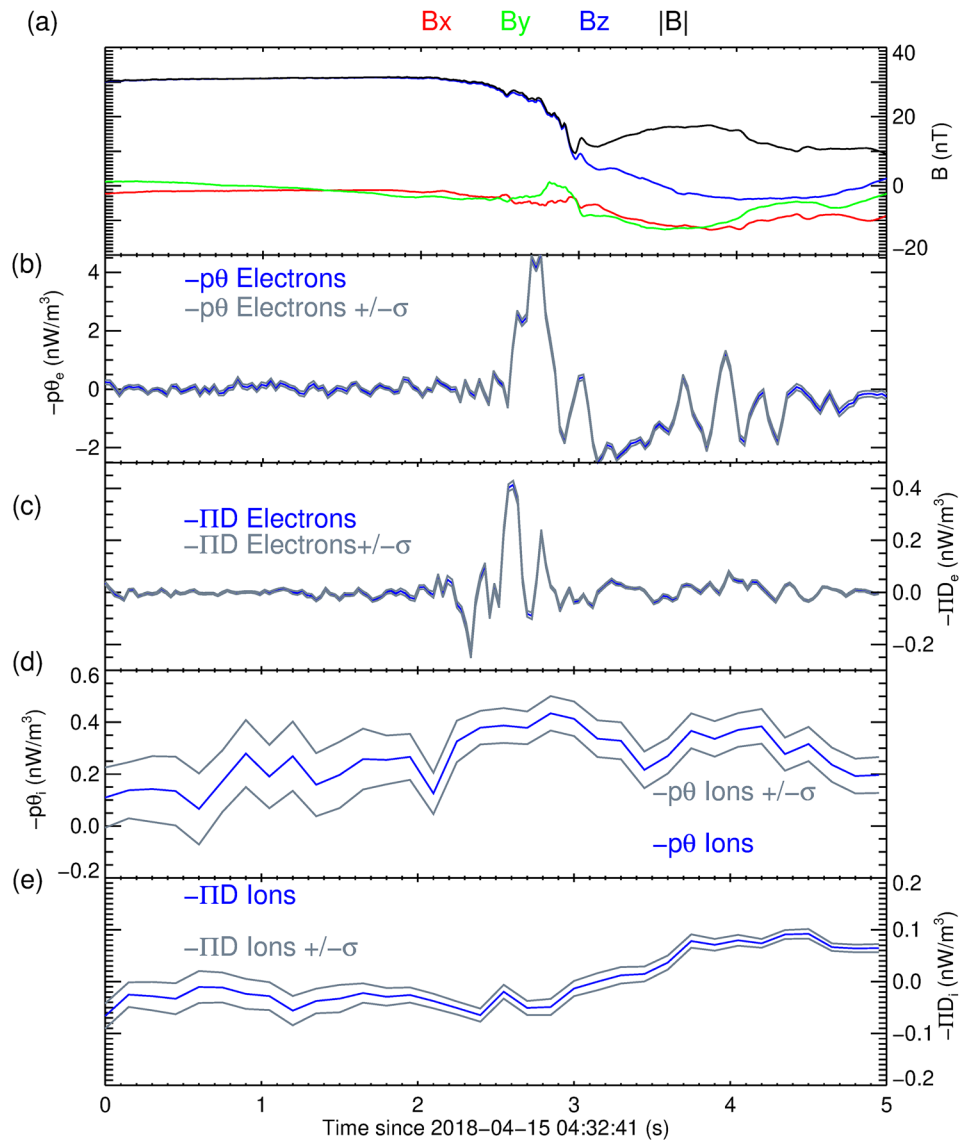


Figure 1. MMS measurements taken during the magnetopause magnetic reconnection event of Burch et al. (2020). (a) Magnetic field measurements from the fluxgate magnetometer in the Geocentric Solar Ecliptic coordinate system. (b) The compressive electron component of the pressure-strain term (c) the incompressible electron component of the pressure-strain term (d) the ion compressive component of the pressure-strain term, and (e) the ion incompressible component. In panels (b–e) blue denotes the measurement, and gray denotes three times the estimated error.

calculating the pressure strain terms. In interval 1 the relative errors on ions and electrons are comparable while in interval 2 the relative error in ions is larger.

5. Summary

To summarize, we have investigated the uncertainties in the pressure strain terms through error propagation and a statistical test. Both approaches yield almost identical results. Relations have been given to estimate the error. The error here is assumed mostly due to Poisson noise in the plasma moments and the tetrahedron shape. The uncertainty due to the spacecraft positions and timing are small. Furthermore, there could be other errors, which we will briefly discuss.

Because of instrument design, there can be an offset in a velocity component between spacecraft; for MMS, this most likely affects the V_z component. This systematic error could cause an additional error in the gradient

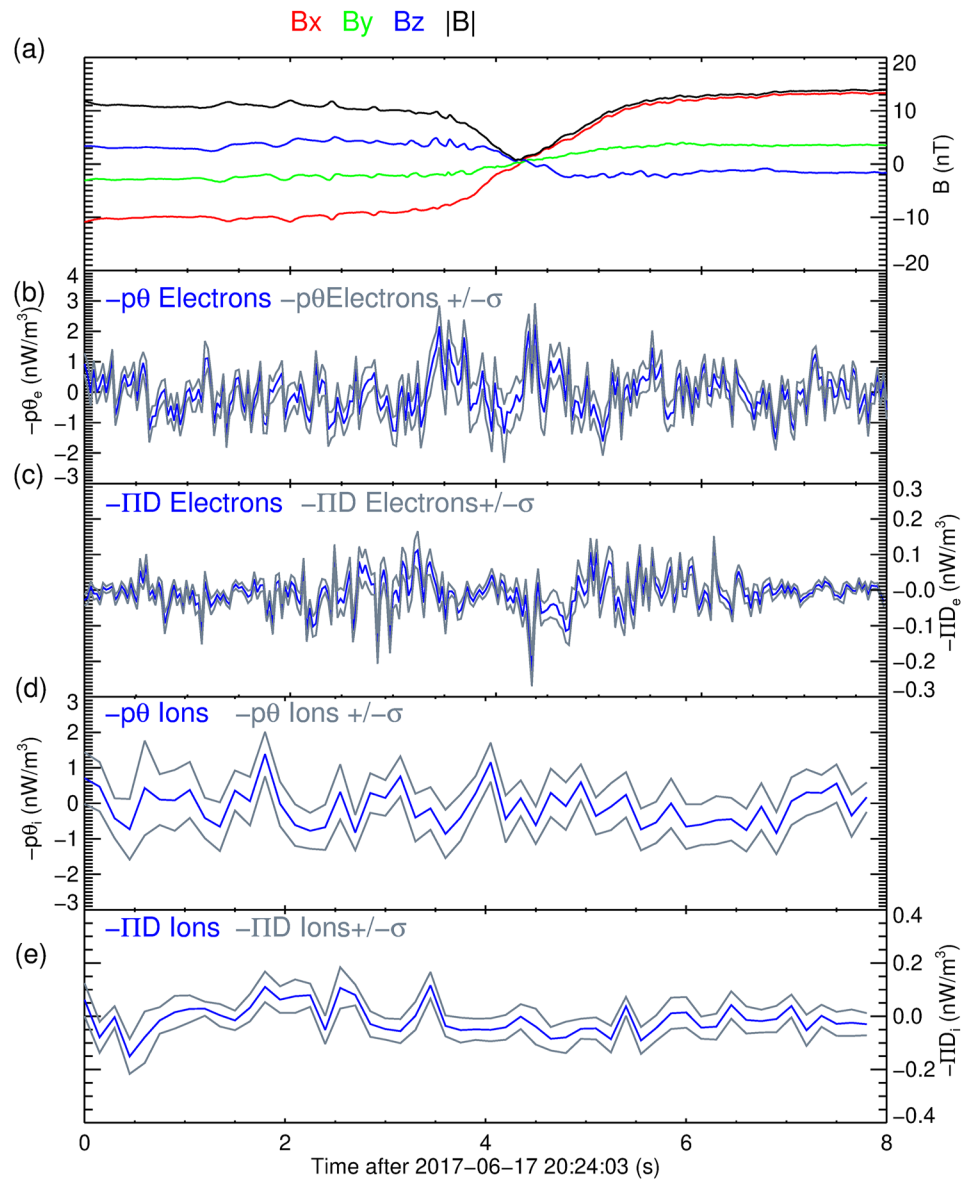


Figure 2. The same as Figure 1 but for the magnetotail event of Lu et al. (2020).

Table 1
Table of the Absolute Errors for Both Cases Studied

	Electrons		Ions	
	$\sigma[p\theta]$ (nW/m ³)	$\sigma[\Pi D]$ (nW/m ³)	$\sigma[p\theta]$ (nW/m ³)	$\sigma[\Pi D]$ (nW/m ³)
Magnetopause ($n = 7.19 \text{ cm}^{-3}$)				
Analytical error propagation	0.087	0.006	0.089	0.017
Resampling method	0.087	0.007	0.089	0.017
Magnetotail ($n = 0.58 \text{ cm}^{-3}$)				
Analytical error propagation	0.425	0.023	0.632	0.05
Resampling method	0.426	0.027	0.628	0.06

Note. Note that the $p\theta$ and ΠD fluctuate quantities around zero, so we do not state the mean of the relative error as this may be undefined when the measured quantity is zero.

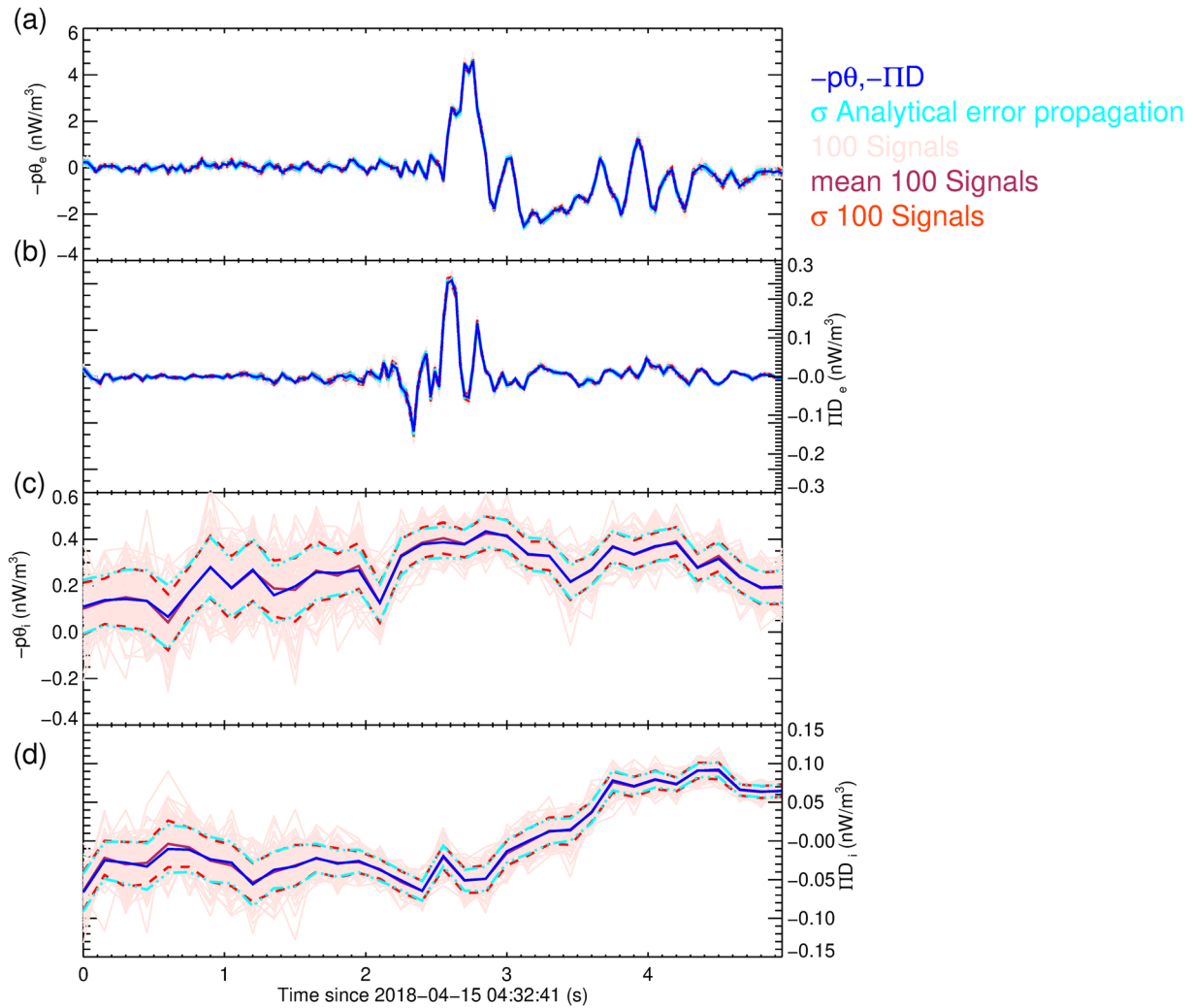


Figure 3. The different electron and ion pressure strain terms for the magnetopause event. Blue denotes the pressure strain terms, and cyan denotes the analytical error. The pink lines denote 100 time series where a random error is introduced (see text), the maroon denotes the mean of these time series (almost identical to the blue curve). The red lines denote the standard deviation of these 100 time series giving an additional estimation of the error, which agrees well with the cyan curves.

measurements. Another possible source of error is related to the spacecraft separations; by calculating a gradient using multiple spacecraft, we are looking at a spatial gradient accurate to a certain scale. Different plasma species have different length scales, so spacecraft separations may be inadequate for measuring the pressure strain interaction for a certain species. Numerical simulations by Matthaeus et al. (2020) and Yang et al. (2022) show scale dependence in the average value of the pressure strain term. At inertial scales, the average of the pressure strain term is small but increases at length scales below the ion inertial length. Thus the relative error at different scales may differ even if the statistical errors on the moments are equal. With MMS, we are limited to electron scale separations where the pressure strain terms are expected to be large. However, comparisons with numerical simulations, or spacecraft data with multiple separations (relative to the ion/electron characteristic scales) would be useful to understand how the spacecraft separations may affect the result (Bandyopadhyay, Matthaeus, Parashar, et al., 2020). This would be especially useful in preparation for HelioSwarm as the nine spacecraft allow multi-scale estimations of the pressure strain terms. Other potential sources of error may come from the calibration, penetrating radiation, spin tones, and effects due to spacecraft charging.

The pressure strain terms show that the energy transfer is highly localized, with significantly larger energy conversion near coherent structures (Bandyopadhyay et al., 2021; Bandyopadhyay, Matthaeus, Parashar, et al., 2020; Chasapis et al., 2018; Yang, Matthaeus, Parashar, Haggerty, et al., 2017). In these localized cases, the relative errors are very small. However, we must consider the error if we consider a more statistical approach as advocated

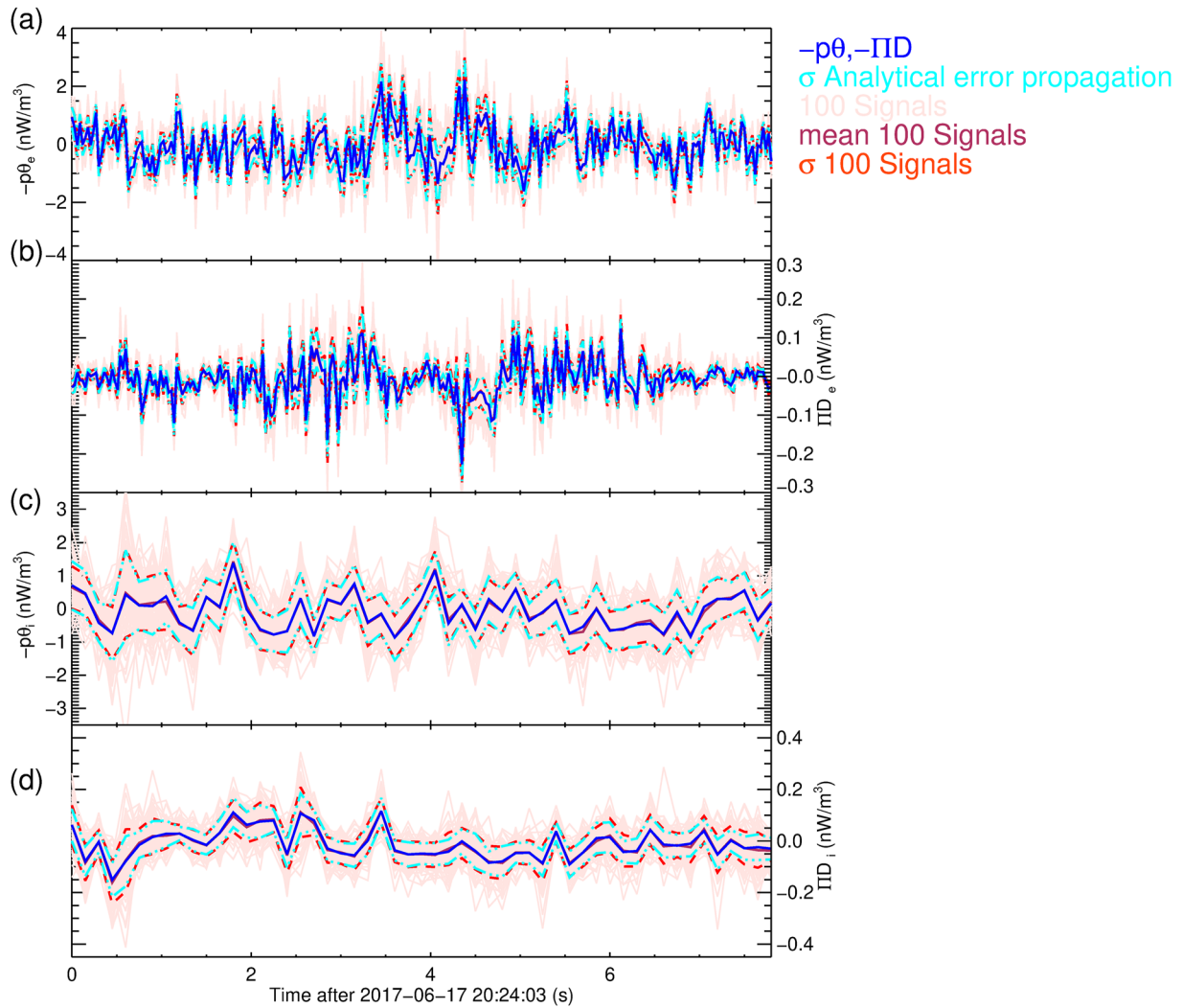


Figure 4. Same as Figure 3 but for the magnetotail case.

in Vörös et al. (2023). If the value of a pressure strain term, considering the error straddles zero, we cannot conclude that there is a net energy transfer. In understanding the energy budget using these measurements, we might wish only to consider cases where $-PS > \sigma[PS]$ and $-PS < -\sigma[PS]$, where we can have some statistical confidence that there is energy conversion. This is similar to (Ergun et al., 2018) has presented in terms of the $J \cdot E$ term.

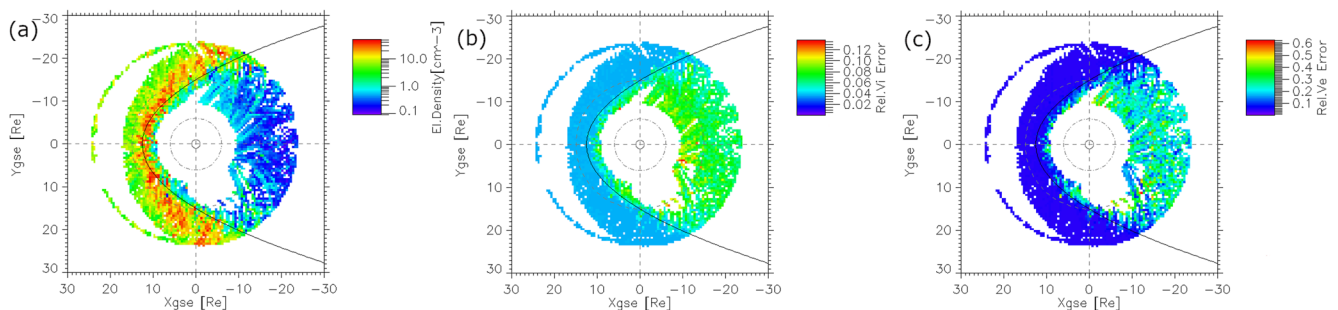


Figure 5. MMS fast survey mode data from 2018 as a function of the spacecraft position in the xy GSE plane. Panel (a) shows the electron density measured by FPI. Panels (b) and (c) show the relative error in the bulk velocity for ions and electrons, respectively.

Two examples in different plasma conditions were presented; the propagated errors at the magnetopause were smaller than the tail, as expected, due to lower counting statistics in the tail. While the errors are generally small, caution should be exercised in low plasma regions, where counting statistics are poor. However, we expect calculating the pressure strain terms in the magnetosheath (high density) to have an excellent signal-to-noise ratio. It should, however, be noted that FPI is not designed for the solar wind and is subject to substantial variations at the spacecraft spin frequency (Bandyopadhyay et al., 2018; Roberts et al., 2021; Wilson III et al., 2022); this method should not be used with MMS in the solar wind.

Appendix A: Estimation of the Inaccuracies in Spacecraft Timing and Position

Here, we give a more quantitative estimate of the errors due to timing accuracy and the spacecraft positions. We estimate the effect by comparing the statistical errors with the product of the gradient and the estimated positional $|\frac{\partial V_x}{\partial r_i}| \sigma[r]$ and timing inaccuracies $|\frac{dV_x}{dt}| \sigma[\text{timing}]$. Where $\sigma[r] = 0.1$ km, $\sigma[\text{timing}] = 1$ ms (Tooley et al., 2016). Table A1 and Table A2 show the mean and maximum values of the gradients and the statistical uncertainties for the x component of the velocity in GSE. Other components have similar values. The values are much smaller than the statistical uncertainties (Vogt et al., 2020), confirming that timing and positional uncertainties are negligible. The different components of velocity all show similar relationships.

Table A1
Table Showing the Product of Different Gradients and the Inaccuracies Due To Position and Timing for Interval 1

	Ions	
	Mean	Max
$ \frac{\partial V_x}{\partial x} \sigma[r]$	0.04	0.08
$ \frac{\partial V_x}{\partial y} \sigma[r]$	0.05	0.09
$ \frac{\partial V_x}{\partial z} \sigma[r]$	0.1	0.2
$ \frac{dV_x}{dt} \sigma[\text{timing}]$	0.003	0.09
$\sigma[V_x]$	4	9
	Electrons	
$ \frac{\partial V_x}{\partial x} \sigma[r]$	0.5	2
$ \frac{\partial V_x}{\partial y} \sigma[r]$	0.3	2
$ \frac{\partial V_x}{\partial z} \sigma[r]$	0.01	6
$ \frac{dV_x}{dt} \sigma[\text{timing}]$	0.01	6
$\sigma[V_x]$	18	56

Table A2
Table Showing the Product of Different Gradients and the Inaccuracies Due To Position and Timing for Interval 2

	Ions	
	Mean	Max
$ \frac{\partial V_x}{\partial x} \sigma[r]$	0.07	0.2
$ \frac{\partial V_x}{\partial y} \sigma[r]$	0.07	0.2
$ \frac{\partial V_x}{\partial z} \sigma[r]$	0.09	0.3
$ \frac{dV_x}{dt} \sigma[\text{timing}]$	0.01	0.4

Table A2
Continued

	Ions	
	Mean	Max
$\sigma[V_x]$	17	66
	Electrons	
$ \frac{\partial V_x}{\partial x} \sigma[r]$	0.8	3
$ \frac{\partial V_x}{\partial y} \sigma[r]$	1	5
$ \frac{\partial V_x}{\partial z} \sigma[r]$	0.8	4
$ \frac{dV_x}{dt} \sigma[\text{timing}]$	0.05	13
$\sigma[V_x]$	89	193

Data Availability Statement

The datasets analyzed for this study can be found in the MMS data archive <https://lasp.colorado.edu/mms/sdc/public/>. We use version 3.3 of the FPI level 2 moments data, version 5 of the fgm data, and version 2 of the ephemeris data. These data are the most recent versions and are loaded using the SPEDAS software (Angelopoulos et al., 2019). Codes for the gradient, divergence and curl calculation from four-point measurements are also publicly available in the SPEDAS package (Angelopoulos et al., 2019), <http://spedas.org/>.

Acknowledgments

OWR gratefully acknowledges the Austrian Science Fund (FWF): P 33285-N for supporting this project. We acknowledge the fluxgate magnetometer and the fast plasma investigation teams for the excellent data MMS provides that makes using such techniques possible. This research was supported by the International Space Science Institute (ISSI) in Bern, through ISSI International Team project #556 (Cross-scale energy transfer in space plasmas). We wish to acknowledge NASA Heliospheric GI Grant 80NSSC21K0739 and NASA Grant 80NSSC21K1458 at Princeton University.

References

- Angelopoulos, V. (2008). The THEMIS mission. *Space Science Reviews*, 141(1–4), 5–34. <https://doi.org/10.1007/s11214-008-9336-1>
- Angelopoulos, V., Cruce, P., Drozdov, A., Grimes, E. W., Hatzigeorgiu, N., King, D. A., et al. (2019). The space physics environment data analysis system (SPEDAS). *Space Science Reviews*, 215(1), 9. <https://doi.org/10.1007/s11214-018-0576-4>
- Bandyopadhyay, R., Chasapis, A., Chhiber, R., Parashar, T. N., Maruca, B. A., Matthaeus, W. H., et al. (2018). Solar wind turbulence studies using MMS fast plasma investigation data. *The Astrophysical Journal*, 866(2), 81. <https://doi.org/10.3847/1538-4357/aade93>
- Bandyopadhyay, R., Chasapis, A., Matthaeus, W. H., Parashar, T. N., Haggerty, C. C., Shay, M. A., et al. (2021). Energy dissipation in turbulent reconnection. *Physics of Plasmas*, 28(11). <https://doi.org/10.1063/5.0071015>
- Bandyopadhyay, R., Matthaeus, W. H., Chasapis, A., Russell, C. T., Strangeway, R. J., Torbert, R. B., et al. (2020). Direct measurement of the solar-wind Taylor microscale using MMS turbulence campaign data. *The Astrophysical Journal*, 899(1), 63. <https://doi.org/10.3847/1538-4357/ab9ebe>
- Bandyopadhyay, R., Matthaeus, W. H., Parashar, T. N., Yang, Y., Chasapis, A., Giles, B. L., et al. (2020). Statistics of kinetic dissipation in the Earth's magnetosheath: MMS observations. *Physical Review Letters*, 124(25), 255101. <https://doi.org/10.1103/PhysRevLett.124.255101>
- Birn, J., & Hesse, M. (2005). Energy release and conversion by reconnection in the magnetotail. *Annales Geophysicae*, 23(10), 3365–3373. <https://doi.org/10.5194/angeo-23-3365-2005>
- Birn, J., & Hesse, M. (2010). Energy release and transfer in guide field reconnection. *Physics of Plasmas*, 17(1), 012109. <https://doi.org/10.1063/1.3299388>
- Broeren, T., Klein, K. G., TenBarge, J. M., Dors, I., Roberts, O. W., & Verscharen, D. (2021). Magnetic field reconstruction for a realistic multi-point, multi-scale spacecraft observatory. *Frontiers in Astronomy and Space Sciences*, 8. <https://doi.org/10.3389/fspas.2021.727076>
- Burch, J. L., Moore, T. E., Torbert, R. B., & Giles, B. L. (2016). Magnetospheric multiscale overview and science objectives. *Space Science Reviews*, 199(1–4), 5–21. <https://doi.org/10.1007/s11214-015-0164-9>
- Burch, J. L., Webster, J. M., Hesse, M., Genestreti, K. J., Denton, R. E., Phan, T. D., et al. (2020). Electron inflow velocities and reconnection rates at Earth's magnetopause and magnetosheath. *Geophysical Research Letters*, 47(17), 1–10. <https://doi.org/10.1029/2020GL089082>
- Cassak, P. A., & Barbhuiya, M. H. (2022). Pressure–strain interaction. I. On compression, deformation, and implications for Pi-D. *Physics of Plasmas*, 29(12), 122306. <https://doi.org/10.1063/5.0125248>
- Cerri, S. S., Califano, F., Jenko, F., Told, D., & Rincon, F. (2016). Subproton-scale cascades in solar wind turbulence: Driven hybrid-kinetic simulations. *The Astrophysical Journal*, 822(1), L12. <https://doi.org/10.3847/2041-8205/822/1/L12>
- Chanteur, G. (1998). Spatial interpolation for four spacecraft: Theory. In *Analysis methods for multi-spacecraft data* (Vol. 14).
- Chanteur, G. (2000). Accuracy of fields gradient estimations by cluster: Explanation of its dependency upon elongation and planarity of the tetrahedron. In *Cluster-ii workshop: Multiscale/multipoint plasma measurements, proceedings of the workshop held at imperial college* (p. 265).
- Chasapis, A., Yang, Y., Matthaeus, W. H., Parashar, T. N., Haggerty, C. C., Burch, J. L., et al. (2018). Energy conversion and collisionless plasma dissipation channels in the turbulent magnetosheath observed by the magnetospheric multiscale mission. *The Astrophysical Journal*, 862(1), 32. <https://doi.org/10.3847/1538-4357/aac775>
- Chen, C. H. K., Horbury, T. S., Schekochihin, A. A., Wicks, R. T., Alexandrova, O., & Mitchell, J. (2010). Anisotropy of solar wind turbulence between ion and electron scales. *Physical Review Letters*, 104(255002), 1–4. <https://doi.org/10.1103/PhysRevLett.104.255002>
- Constantinescu, O. (2007). Wave sources and structures in the Earth's magnetosheath and adjacent regions (doctoral dissertation).
- Del Sarto, D., & Pegoraro, F. (2018). Shear-induced pressure anisotropization and correlation with fluid vorticity in a low collisionality plasma. *Monthly Notices of the Royal Astronomical Society*, 475(1), 181–192. <https://doi.org/10.1093/mnras/stx3083>

- Del Sarto, D., Pegoraro, F., & Califano, F. (2016). Pressure anisotropy and small spatial scales induced by velocity shear. *Physical Review E*, 93(5), 053203. <https://doi.org/10.1103/PhysRevE.93.053203>
- Denton, R. E., Liu, Y., Hasegawa, H., Torbert, R. B., Li, W., Fuselier, S., & Burch, J. L. (2022). Polynomial reconstruction of the magnetic field observed by multiple spacecraft with integrated velocity determination. *Journal of Geophysical Research: Space Physics*, 127(10), e2022JA030512. <https://doi.org/10.1029/2022JA030512>
- Denton, R. E., Torbert, R. B., Hasegawa, H., Dors, I., Genestreti, K. J., Argall, M. R., et al. (2020). Polynomial reconstruction of the reconnection magnetic field observed by multiple spacecraft. *Journal of Geophysical Research: Space Physics*, 125(2), 1–52. <https://doi.org/10.1029/2019ja027481>
- Dudok de Wit, T., Bale, S., Krasnosel'skikh, V. V., Dunlop, M. W., Lühr, H., Woolliscroft, L. J. C., & Schwartz, S. J. (1995). Determination of dispersion relations in quasi-stationary plasma turbulence using dual satellite data. *Geophysical Research Letters*, 22(19), 2653–2656. <https://doi.org/10.1029/95gl02543>
- Dunlop, M., Southwood, D., Glassmeier, K.-H., & Neubauer, F. (1988). Analysis of multipoint magnetometer data. *Advances in Space Research*, 8(9–10), 273–277. [https://doi.org/10.1016/0273-1177\(88\)90141-X](https://doi.org/10.1016/0273-1177(88)90141-X)
- Dunlop, M. W., Balogh, A., Glassmeier, K.-H., & Robert, P. (2002). Four-point Cluster application of magnetic field analysis tools: The Curlometer. *Journal of Geophysical Research*, 107(A11), 1–14. <https://doi.org/10.1029/2001JA005088>
- Dunlop, M. W., Dong, X. C., Wang, T. Y., Eastwood, J. P., Robert, P., Haaland, S., et al. (2021). Curlometer technique and applications. *Journal of Geophysical Research: Space Physics*, 126(11), e2021JA029538. <https://doi.org/10.1029/2021JA029538>
- Ergun, R. E., Goodrich, K. A., Wilder, F. D., Ahmadi, N., Holmes, J. C., Eriksson, S., et al. (2018). Magnetic reconnection, turbulence, and particle acceleration: Observations in the Earth's magnetotail. *Geophysical Research Letters*, 45(8), 3338–3347. <https://doi.org/10.1002/2018GL076993>
- Escoubet, C. P., Fehringer, M., & Goldstein, M. (2001). Introduction the cluster mission. *Annales Geophysicae*, 19(10/12), 1197–1200. <https://doi.org/10.5194/angeo-19-1197-2001>
- Escoubet, C. P., Schmidt, R., & Goldstein, M. (1997). Cluster – Science and mission overview. *Space Science Reviews*, 79(1–2), 11–32. <https://doi.org/10.1023/a:1004923124586>
- Fadanelli, S., Lavraud, B., Califano, F., Cozzani, G., Finelli, F., & Sisti, M. (2021). Energy conversions associated with magnetic reconnection. *Journal of Geophysical Research: Space Physics*, 126(1), 1–12. <https://doi.org/10.1029/2020JA028333>
- Friis-Christensen, E., Lühr, H., Knudsen, D., & Haagmans, R. (2008). Swarm – An Earth observation mission investigating geospace. *Advances in Space Research*, 41(1), 210–216. <https://doi.org/10.1016/j.asr.2006.10.008>
- Gershman, D. J., Avakov, L. A., Boardsen, S. A., Dorelli, J. C., Gliese, U., Barrie, A. C., et al. (2017). Spacecraft and instrument photoelectrons measured by the dual electron spectrometers on MMS. *Journal of Geophysical Research: Space Physics*, 122(11), 11548–11558. <https://doi.org/10.1002/2017JA024518>
- Gershman, D. J., Dorelli, J. C., F-Viñas, A., & Pollock, C. J. (2015). The calculation of moment uncertainties from velocity distribution functions with random errors. *Journal of Geophysical Research: Space Physics*, 120(8), 6633–6645. <https://doi.org/10.1002/2014JA020775>
- Gershman, D. J., F-Viñas, A., Dorelli, J. C., Goldstein, M. L., Shuster, J., Avakov, L. A., et al. (2018). Energy partitioning constraints at kinetic scales in low- β turbulence. *Physics of Plasmas*, 25(2), 022303. <https://doi.org/10.1063/1.5009158>
- Glassmeier, K.-H., Motschmann, U., Dunlop, M., Balogh, A., Acuña, M. H., Carr, C., et al. (2001). Cluster as a wave telescope – First results from the fluxgate magnetometer. *Annales Geophysicae*, 19(10/12), 1439–1447. <https://doi.org/10.5194/angeo-19-1439-2001>
- Horbury, T. (2000). Cluster II analysis of turbulence using correlation functions. In *Cluster-ii workshop: Multiscale/multipoint plasma measurements* (pp. 89–97).
- Kieokaew, R., & Foullon, C. (2019). Kelvin-Helmholtz waves magnetic curvature and vorticity: Four-spacecraft cluster observations. *Journal of Geophysical Research: Space Physics*, 124(5), 3347–3359. <https://doi.org/10.1029/2019JA026484>
- Klein, K. G., Alexandrova, O., Bookbinder, J., Caprioli, D., Case, A. W., Chandran, B. D. G., et al. (2019). [Plasma 2020 decadal] multipoint measurements of the solar wind: A proposed advance for studying magnetized turbulence. <https://doi.org/10.48550/arXiv.1903.05740>
- Lavraud, B., & Larson, D. E. (2016). Correcting moments of in situ particle distribution functions for spacecraft electrostatic charging. *Journal of Geophysical Research: Space Physics*, 121(9), 8462–8474. <https://doi.org/10.1002/2016JA022591>
- Lavraud, B., Zhang, Y. C., Vernisse, Y., Gershman, D. J., Dorelli, J., Cassak, P. A., et al. (2016). Currents and associated electron scattering and bouncing near the diffusion region at Earth's magnetopause. *Geophysical Research Letters*, 43(7), 3042–3050. <https://doi.org/10.1002/2016GL068359>
- Lu, S., Wang, R., Lu, Q., Angelopoulos, V., Nakamura, R., Artemyev, A. V., et al. (2020). Magnetotail reconnection onset caused by electron kinetics with a strong external driver. *Nature Communications*, 11(1), 1–7. <https://doi.org/10.1038/s41467-020-18787-w>
- Matthaeus, W. H. (2021). Turbulence in space plasmas: Who needs it? *Physics of Plasmas*, 28(3), 032306. <https://doi.org/10.1063/5.0041540>
- Matthaeus, W. H., Dasso, S., Weygand, J. M., Milano, L. J., Smith, C. W., & Kivelson, M. G. (2005). Spatial correlation of solar-wind turbulence from two-point measurements. *Physical Review Letters*, 95(23), 231101. <https://doi.org/10.1103/PhysRevLett.95.231101>
- Matthaeus, W. H., Yang, Y., Wan, M., Parashar, T. N., Bandyopadhyay, R., Chasapis, A., et al. (2020). Pathways to dissipation in weakly collisional plasmas. *The Astrophysical Journal*, 891(1), 101. <https://doi.org/10.3847/1538-4357/ab6d6a>
- Motschmann, U., Woodward, T. I., Glassmeier, K. H., Southwood, D. J., & Pinçon, J. L. (1996). Wavelength and direction filtering by magnetic measurements at satellite arrays: Generalized minimum variance analysis. *Journal of Geophysical Research*, 101(A3), 4961–4965. <https://doi.org/10.1029/95JA03471>
- Narita, Y., Glassmeier, K.-H., & Motschmann, U. (2010). Wave vector analysis methods using multi-point measurements. *Nonlinear Processes in Geophysics*, 17(5), 383–394. <https://doi.org/10.5194/npg-17-383-2010>
- Narita, Y., Glassmeier, K.-H., & Motschmann, U. (2011). High-resolution wave number spectrum using multi-point measurements in space – The multi-point signal resonator (MSR) technique. *Annales Geophysicae*, 29(2), 351–360. <https://doi.org/10.5194/angeo-29-351-2011>
- Narita, Y., Plaschke, F., & Vörös, Z. (2021). The magnetosheath (pp. 137–152). <https://doi.org/10.1002/9781119815624.ch9>
- Osman, K., & Horbury, T. (2009). Quantitative estimates of the slab and 2-D power in solar wind turbulence using multispacecraft data. *Journal of Geophysical Research*, 114(A06103), 1–8. <https://doi.org/10.1029/2008JA014036>
- Osman, K. T., & Horbury, T. S. (2007). Multispacecraft measurement of anisotropic correlation functions in solar wind turbulence. *The Astrophysical Journal*, 654(1), L103–L106. <https://doi.org/10.1086/510906>
- Paschmann, G. (1998). In G. Paschmann (Ed.), *Analysis methods for multi-spacecraft data*.
- Paschmann, G., & Daly, P. (2008). Multi-spacecraft analysis methods revisited.
- Pecora, F., Servidio, S., Primavera, L., Greco, A., Yang, Y., & Matthaeus, W. H. (2023). Multipoint turbulence analysis with HelioSwarm. *The Astrophysical Journal Letters*, 945(2), L20. <https://doi.org/10.3847/2041-8213/acbb03>
- Perri, S., Valentini, F., Sorriso-Valvo, L., Reda, A., & Malara, F. (2017). On the estimation of the current density in space plasmas: Multi- versus single-point techniques. *Planetary and Space Science*, 140, 6–10. <https://doi.org/10.1016/j.pss.2017.03.008>

- Perrone, D., Alexandrova, O., Mangeney, A., Maksimovic, M., Lacombe, C., Rakoto, V., et al. (2016). Compressive coherent structures at ion scales in the slow solar wind. *The Astrophysical Journal*, 826(2), 196. <https://doi.org/10.3847/0004-637X/826/2/196>
- Perrone, D., Alexandrova, O., Roberts, O. W., Lion, S., Lacombe, C., Walsh, A., et al. (2017). Coherent structures at ion scales in fast solar wind: Cluster observations. *The Astrophysical Journal*, 849(1), 49. <https://doi.org/10.3847/1538-4357/aa9022>
- Pezzi, O., Yang, Y., Valentini, F., Servidio, S., Chasapis, A., Matthaeus, W. H., & Veltri, P. (2019). Energy conversion in turbulent weakly collisional plasmas: Eulerian hybrid Vlasov-Maxwell simulations. *Physics of Plasmas*, 26(7), 1–11. <https://doi.org/10.1063/1.5100125>
- Phan, T. D., Eastwood, J. P., Cassak, P. A., Øieroset, M., Gosling, J. T., Gershman, D. J., et al. (2016). MMS observations of electron-scale filamentary currents in the reconnection exhaust and near the X line. *Geophysical Research Letters*, 43(12), 6060–6069. <https://doi.org/10.1002/2016GL069212>
- Pincon, J., & Lefeuvre, F. (1991). Local characterization of homogeneous turbulence in a space plasma from simultaneous measurements of field components at several points in space. *Journal of Geophysical Research*, 96(A2), 1789–1802. <https://doi.org/10.1029/90ja02183>
- Pollock, C., Moore, T., Jacques, A., Burch, J., Gliese, U., Saito, Y., et al. (2016). Fast plasma investigation for magnetospheric multiscale. *Space Science Reviews*, 199(1–4), 331–406. <https://doi.org/10.1007/s11214-016-0245-4>
- Robert, P., Dunlop, M. W., Roux, A., & Chanteur, G. (1998). Accuracy of current density determination. *Analysis Methods for Multi-Spacecraft Data*, 001, 395–418.
- Robert, P., Roux, A., Harvey, C., Dunlop, M., Daly, P., & Glassmeier, K.-H. (1998). Tetrahedron geometric factors. In P. Paschmann & G. Daly (Eds.), *Analysis methods for multi-spacecraft data* (pp. 323–348).
- Roberts, O. W., Alexandrova, O., Sorriso-Valvo, L., Vörös, Z., Nakamura, R., Fischer, D., et al. (2022). Scale-dependent kurtosis of magnetic field fluctuations in the solar wind: A multi-scale study with cluster 2003–2015. *Journal of Geophysical Research: Space Physics*, 127(9), 1–25. <https://doi.org/10.1029/2021JA029483>
- Roberts, O. W., Li, X., & Jeska, L. (2014). Validation of the k-filtering technique for a signal composed of random phase plane waves and non-random coherent structures. *Geoscientific Information and Data Systems*, 3(2), 247–254. <https://doi.org/10.5194/gi-3-247-2014>
- Roberts, O. W., Nakamura, R., Coffey, V. N., Gershman, D. J., Volwerk, M., Varsani, A., et al. (2021). A study of the solar wind ion and electron measurements from the magnetospheric multiscale mission's fast plasma investigation. *Journal of Geophysical Research: Space Physics*, 126(10), 1–18. <https://doi.org/10.1029/2021ja029784>
- Roberts, O. W., Narita, Y., Li, X., Escoubet, C. P., & Laakso, H. (2017). Multipoint analysis of compressive fluctuations in the fast and slow solar wind. *Journal of Geophysical Research: Space Physics*, 122(7), 6940–6963. <https://doi.org/10.1002/2016JA023552>
- Russell, C. T., Anderson, B. J., Baumjohann, W., Bromund, K. R., Dearborn, D., Fischer, D., et al. (2016). The magnetospheric multiscale magnetometers. *Space Science Reviews*, 199(1–4), 189–256. <https://doi.org/10.1007/s11214-014-0057-3>
- Toole, C. R., Black, R. K., Robertson, B. P., Stone, J. M., Pope, S. E., & Davis, G. T. (2016). The magnetospheric multiscale constellation. *Space Science Reviews*, 199(1–4), 23–76. <https://doi.org/10.1007/s11214-015-0220-5>
- Vogt, J., Albert, A., & Marghito, O. (2009). Analysis of three-spacecraft data using planar reciprocal vectors: Methodological framework and spatial gradient estimation. *Annales Geophysicae*, 27(8), 3249–3273. <https://doi.org/10.5194/angeo-27-3249-2009>
- Vogt, J., Blagau, A., & Pick, L. (2020). Robust Adaptive spacecraft array derivative analysis. *Earth and Space Science*, 7(3). <https://doi.org/10.1029/2019EA000953>
- Vogt, J., Haaland, S., & Paschmann, G. (2011). Accuracy of multi-point boundary crossing time analysis. *Annales Geophysicae*, 29(12), 2239–2252. <https://doi.org/10.5194/angeo-29-2239-2011>
- Vogt, J., Narita, Y., & Constantinescu, O. (2008). The wave surveyor technique for fast plasma wave detection in multi-spacecraft data. *Annales Geophysicae*, 26(7), 1699–1710. <https://doi.org/10.5194/angeo-26-1699-2008>
- Vogt, J., & Paschmann, G. (1998). Accuracy of plasma moment derivatives. In G. Paschmann & P. Daly (Eds.), *Analysis methods for multi-spacecraft data* (Vol. 17).
- Vogt, J., Paschmann, G., & Chanteur, G. (2008). Reciprocal vectors. In G. Paschmann & P. Daly (Eds.), *Multi-spacecraft analysis methods revisited*.
- Vörös, Z., Roberts, O. W., Yordanova, E., Sorriso-Valvo, L., Nakamura, R., Narita, Y., et al. (2023). How to improve our understanding of solar wind-magnetosphere interactions on the basis of the statistical evaluation of the energy budget in the magnetosheath? *Frontiers in Astronomy and Space Sciences*, 10, 1–8. <https://doi.org/10.3389/fspas.2023.1163139>
- Wang, T., Alexandrova, O., Perrone, D., Dunlop, M., Dong, X., Bingham, R., et al. (2019). Magnetospheric multiscale observation of kinetic signatures in the Alfvén vortex. *The Astrophysical Journal*, 871(2), L22. <https://doi.org/10.3847/2041-8213/aafe0d>
- Wilson, L. B., III, Goodrich, K. A., Turner, D. L., Cohen, I. J., Whittlesey, P. L., & Schwartz, S. J. (2022). The need for accurate measurements of thermal velocity distribution functions in the solar wind. *Frontiers in Astronomy and Space Sciences*, 9. <https://doi.org/10.3389/fspas.2022.1063841>
- Yang, Y., Matthaeus, W. H., Parashar, T. N., Haggerty, C. C., Roytershteyn, V., Daughton, W., et al. (2017). Energy transfer, pressure tensor, and heating of kinetic plasma. *Physics of Plasmas*, 24(7), 072306. <https://doi.org/10.1063/1.4990421>
- Yang, Y., Matthaeus, W. H., Parashar, T. N., Wu, P., Wan, M., Shi, Y., et al. (2017). Energy transfer channels and turbulence cascade in Vlasov-Maxwell turbulence. *Physical Review E*, 95(6), 061201. <https://doi.org/10.1103/PhysRevE.95.061201>
- Yang, Y., Matthaeus, W. H., Roy, S., Roytershteyn, V., Parashar, T. N., Bandyopadhyay, R., & Wan, M. (2022). Pressure–Strain interaction as the energy dissipation estimate in collisionless plasma. *The Astrophysical Journal*, 929(2), 142. <https://doi.org/10.3847/1538-4357/ac5d3e>
- Zhang, L. Q., Lui, A. T., Baumjohann, W., Wang, C., Burch, J. L., & Khotyaintsev, Y. V. (2020). Anisotropic vorticity within bursty bulk flow turbulence. *Journal of Geophysical Research: Space Physics*, 125(10), 1–9. <https://doi.org/10.1029/2020JA028255>